WIND VELOCITY MEASUREMENT ACCURACY WITH HIGHLY STABLE 12 mJ/PULSE HIGH REPETITION RATE CO_2 LASER MASTER OSCILLATOR POWER AMPLIFIER

James W. Bilbro and Steven C. Johnson
Marshall Space Flight Center, AL

Jeffry Rothermel
University Space Research Associates
Huntsville, Alabama

SUMMARY

A coherent CO2 lidar operating in a master oscillator power amplifer configuration (MOPA) is described for both ground-based and airborne operation. Representative data taken from measurements against stationary targets in both the ground-based and airborne configurations are shown for the evaluation of the frequency stability of the system. Examples of data are also given which show the results of anomalous system operation. Overall results demonstrate that velocity measurements can be performed consistently to an accuracy of ±0.5 m/s and in some cases ±0.1 m/s.

INTRODUCTION

The pulsed coherent CO_2 lidar is shown in figure 1. This system has been operated in both ground-based and airborne configurations since 1971. Extensive modifications have been made and numerous measurements have been performed to obtain better understanding of the operation of the lidar and its inherent measurement accuracy. Ideally, the measurement accuracy should be determined primarily by the signal-to-noise ratio. To that end, many contributing errors must be overcome. Since many of the errors are due in part to system configuration, the ground-based operation of the system will be described first, followed by a description of airborne operation. A more detailed description of the system, its operation and associated errors will be found in references 1 and 2.

GROUND-BASED CONFIGURATION

A simplified block diagram of the lidar in its ground-based configuration is shown in figure 2. The master oscillator laser is an eight watt continuous wave CO_2 laser operating at a wavelength of 10.6 microns. Briefly, a small portion of the laser output is split off and directed to a pyroelectric detector where it is combined with the local oscillator laser. The beat signal out of this detector is used in a locking loop to lock the

local oscillator laser to a 10 MHz offset from the master oscillator laser. The main portion of the master oscillator laser is directed through an electro-optic modulator, an isolator, a beam expander and into a series of six longitudinal discharge tubes which serve as the power amplifier. The output of the power amplifier passes through a Brewster window, a quarter-wave plate and into the telescope where it is expanded to a diameter of 24 cm (measured to the 1/e2 points). The return beam, scattered by the target, is collected by the same telescope, directed through the quarter-wave plate, then reflected off the Brewster window to the detector where it is combined with the local oscillator beam. The output of the detector is then processed to extract the Doppler velocity and associated information. Velocity errors arise primarily from four different areas within this process. These are discussed in greater detail as follows.

A. Electro-optic modulator

The electro-optic modulator consists of two Cadmium Teluride crystals nested in a series of Brewster plates. Modulation of the beam is accomplished by applying a voltage to the first crystal which rotates the polarization of the beam such that it is passed by the central Brewster plates. At a selectable time later (1, 2, 4, or 8 microseconds), voltage is applied to the second crystal which rotates the polarization so that the beam is blocked by the final set of Brewster plates. Failure of the second crystal in the 1984 flight tests described in reference 1 produced the pulse shape shown in figure 3. The arrow at the top of the figure indicates the point at which the second crystal would normally have terminated the pulse. The exponential decay following the arrow is the relaxation of the crystal while the long tail is the result of acoustic ringing. An amplitude plot of the return in the vicinity of a mountain peak is shown in figure 4. Five traces are shown in this figure, one up wind of the mountain where there are no aerosols and hence no signal, one on the downwind side where aerosols from the mountain have been entrained and three traces where the mountain was hit. The shelf, which is evident just prior to the peak in signal return from the mountain, is due to pre-pulse leakage, whereas the ringing after the peak is due to the pulse tail caused by acoustic ringing in the first crystal. It is apparent that significant errors can result due to contributions from both the pre-pulse shelf and the tail. While it is not evident from looking at the trace of the aerosol return, the apparent range to which measurements have been made has been greatly extended due primarily to the integrating effect of the long tail in particular. Hence, velocity measurements beyond approximately 8 km are in reality the results of an average over the entire length of the tail and are not from the primary pulse. Refurbishment of the modulator with improved mounting techniques has reduced this problem, but a double crystal is still used to provide a well-defined pulse shape. The modulation frequency is variable from 100 to 200 Hz.

B. Isolator

The isolator is an Indium Antimonide crystal embedded in a permanent magnet. The isolator prevents radiation which has been scattered from optical surfaces downstream from the master oscillator from reentering the laser and causing frequency pulling in the master oscillator. The isolator provides approximately 12 dB of isolation with 3 dB of loss. A plot of the apparent Doppler velocity of a mountain approximately 15 km from the lidar with the isolator removed is shown in figure 5. As can be seen from this plot, significant velocity excursions occur with a periodicity of approximately 90 seconds. This is in contrast to the plot shown in figure 6 with the isolator in place. In this case the velocity excursions are less than ±0.5 m/s.

C. Local oscillator

The primary difference between the airborne and ground-based configurations is that in the case of the ground-based configuration, a separate local oscillator laser is locked to the master oscillator laser at a frequency offset of 10 MHz. This allows the velocity sense (i.e., the direction of the motion) to be determined by noting on which side of the 10 MHz local oscillator the Doppler shifter signal occurs. In the offset local oscillator case, error is a function of how well the two lasers can be locked. The locking loop is designed for ±100 kHz; however, in practice considerable variability is experienced depending upon how well the locking loop is tuned under a given set of ambient conditions. Figure 7 shows velocity measurements of the signal return from a mountain at a range of 4350 meters. In this figure, the locking loop has been tuned to produce a variation of only ±0.1 m/s. This corresponds to a frequency stability of approximately ±18 kHz; however, this is the result of a 50 pulse average. If we allow for a n improvement in variance, where n is the number of shots averaged, this results in a single pulse frequency stability of ±50 kHz. Figure 8 illustrates momentary loss of lock resulting in sharp excursions in the measured velocity. A 30 minute time history is shown in figure 9, demonstrating the long-term stability of the system. The slight offset from zero is a function of how well the loop has been tuned to the 10 MHz offset. As can be seen from this figure there is a long-term drift of approximately 0.25 m/s plus occasional short-term oscillations of ±0.25 m/s. Excluding the momentary losses of lock, the overall accuracy of the measurement is determined by the short-term oscillations of ±0.25 m/s.

D. Zero Doppler shift measurement

Ordinarily it is not possible to perform measurements of a stationary target with a coherent lidar such as has been described. This is due to the fact that leakage from the master oscillator laser heterodynes with the local oscillator to produce an extremely strong beat signal at the offset frequency. This beat signal will obscure any return from a stationary target

which also occurs at the offset frequency. Therefore, in order to perform the measurements previously described, it is necessary to remove the offending beat signal. This is accomplished by applying a voltage "kick" to the pzt of the master oscillator laser shortly after pulse transmission. When this occurs, the frequency of the laser is driven to a point where the beat signal between the master oscillator and the local oscillator is outside the bandpass of the signal processing electronics. Scattered radiation from stationary targets will then be heterodyned with the local oscillator and will appear as a beat signal at the offset frequency without contamination from the master oscillator leakage. If this process is not done carefully, errors will be introduced into the measurements. Figure 10 illustrates the frequency excursion of the master oscillator laser as it is driven out of band. It is apparent from this figure that if the master oscillator laser is not driven sufficiently far off, frequency and oscillations appear at the edge of the pass band of the signal processing electronics creating large errors in velocity measurement.

AIRBORNE CONFIGURATION

The primary difference in the basic lidar configuration between ground-based and airborne operation is that instead of using an offset local oscillator, a portion of the master oscillator is used as a local oscillator in a homodyne configuration as shown in figure 11. In the airborne case there is no need to have an offset local oscillator. The Doppler shift due to the aircraft provides the offset necessary to determine the sense of the wind velocity. There are, however, additional factors contributing to the error in that the velocity of the aircraft must be known as well as the attitude of the lidar and the pointing accuracy of the scanner. All of these factors are critical to the wind measurement accuracy.

In operation, an inertial platform is attached directly to the lidar, and the entire assembly is shock mounted to the aircraft. The data from the inertial platform (i.e. pitch, roll, drift angle and true heading, true airspeed) are transmitted to a central computer which calculates the desired scanner settings for pointing the lidar beam. The resulting scanner settings, along with ground speed and true airspeed, are then used to calculate the wind velocity relative to the ground. Typically, the lidar beam is scanned forward 20 degrees and then aft 20 degrees in a horizontal plane at the altitude of the aircraft. This is depicted in figure 12. Data are collected for each range gate of the lidar and averaged for 50 pulses. As can be seen from this figure, each aft scan intersects a number of prior forward scans. At each intersection point a vector velocity can be calculated. The results of such a calculation in a uniform flow field are shown in figure 13. Relative accuracy on the order of 0.2 m/s has been calculated in similar conditions by comparing adjacent

forward scans for variations in velocity measurements. The absolute accuracy of the airborne measurements can be determined by examining ground hits when the beam is given a slight angle of depression. This case is shown in figure 14, where adjacent forward scans are displayed. These scans have a 3-degree depression angle, and the ground hits can be clearly seen as a narrow line separated from the wind data. These ground hits were isolated by amplitude discrimination and their velocity plotted as a function of time. The result is shown in figure 15. Large excursions on the order of 2.0 m/s can be seen in this data. These excursions correspond to heading changes of the aircraft. Extensive investigations are under way to determine the cause of these excursions, but so far no satisfactory explanation has been found. The most likely cause currently under study concerns the potential misalignment due to increased g-loading during aircraft bank. Error in ground speed calculation by the inertial platform may also be a contributor in some cases. In spite of the undesirable excursions, the velocity variation in those time periods between heading changes is quite satisfactory. The time segment from 22:30 to 23:00 is shown expanded in figure 16. In this case the variation is less than ±0.5 m/s which is on the order of the accuracy obtained in ground-based operation.

CONCLUDING REMARKS

A number of examples have been given of the various errors which can occur in coherent lidar data from the instrument standpoint. It is hoped that these examples will serve as a demonstration of the care that must be taken in interpreting data from such an instrument since these errors can often times be mistaken for real data. In addition to the areas addressed, there are significant problems involved in taking into account the various atmospheric effects as well as the different methods of signal processing. While all of these problems are difficult and extreme care must be taken in dealing with them, coherent lidars can provide highly accurate velocity data and can serve as a very useful tool for performing atmospheric research.

REFERENCES

1. Bilbro, J.; DiMarzio, C.; Fitzjarrald, D.; Johnson, S.; Jones, W.: Airborne Doppler Lidar Measurements. Appl. Opt. Nov. 1, 1986.

2. McCaul, Eugene W.,Jr.; Bluestein, Howard B.; and Doviak, Richard J.: Airborne Doppler Lidar Techniques for Observing Severe Thunderstorms. Appl. Opt., Vol. 25, p.698 Mar. 1, 1986.

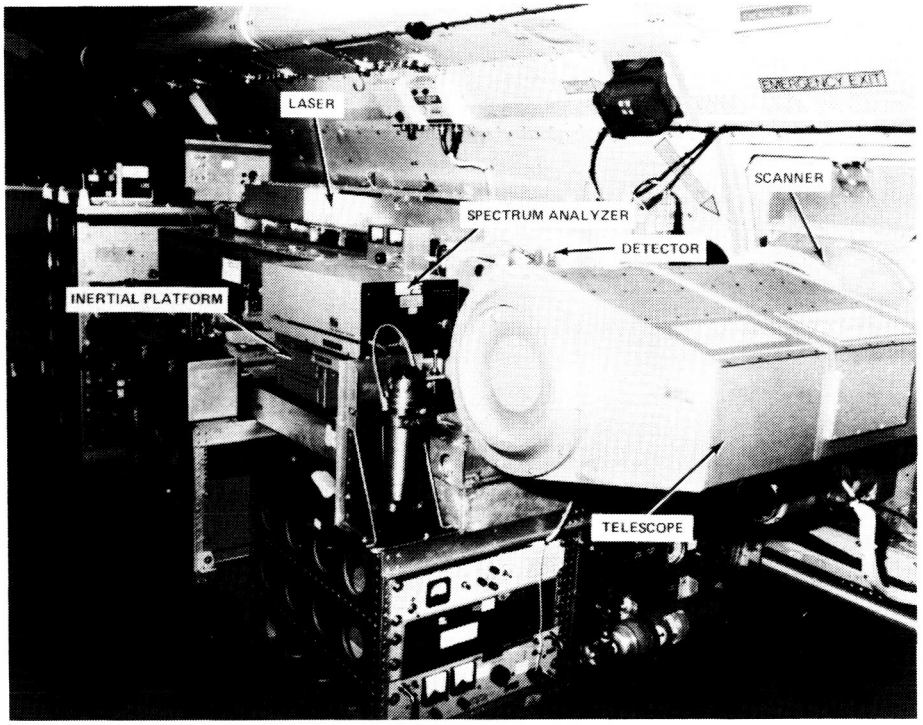

Figure 1. PULSED COHERENT CO_2 LIDAR.

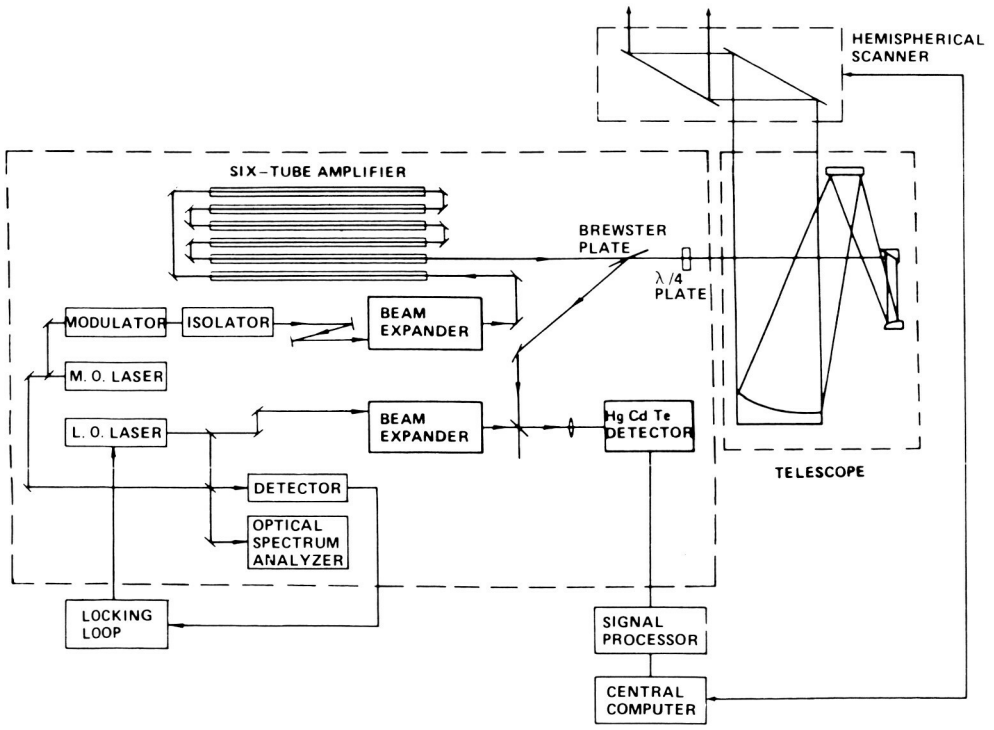

Figure 2. SIMPLIFIED BLOCK DIAGRAM OF GROUND-BASED CONFIGURATION.

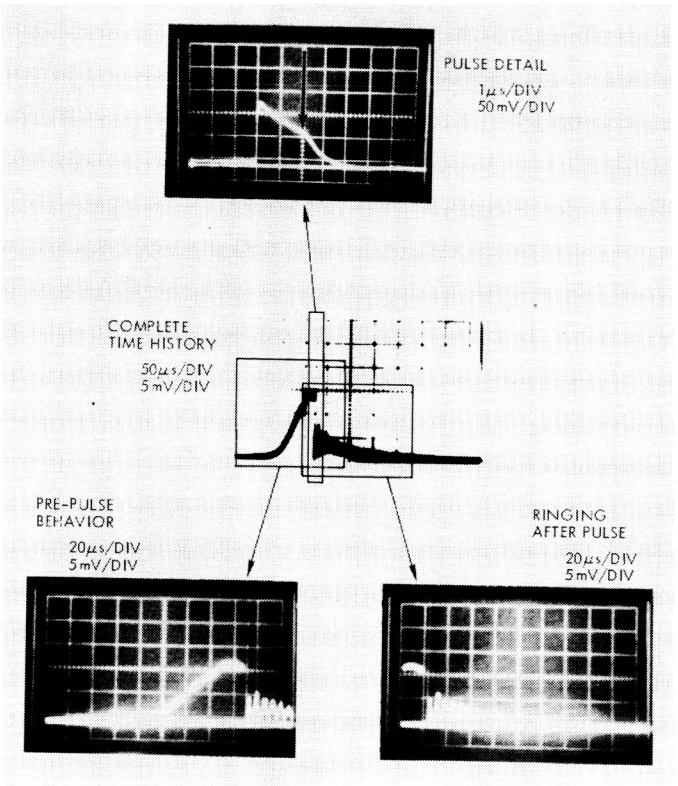

Figure 3. PULSE SHAPE DUE TO MODULATOR FAILURE.

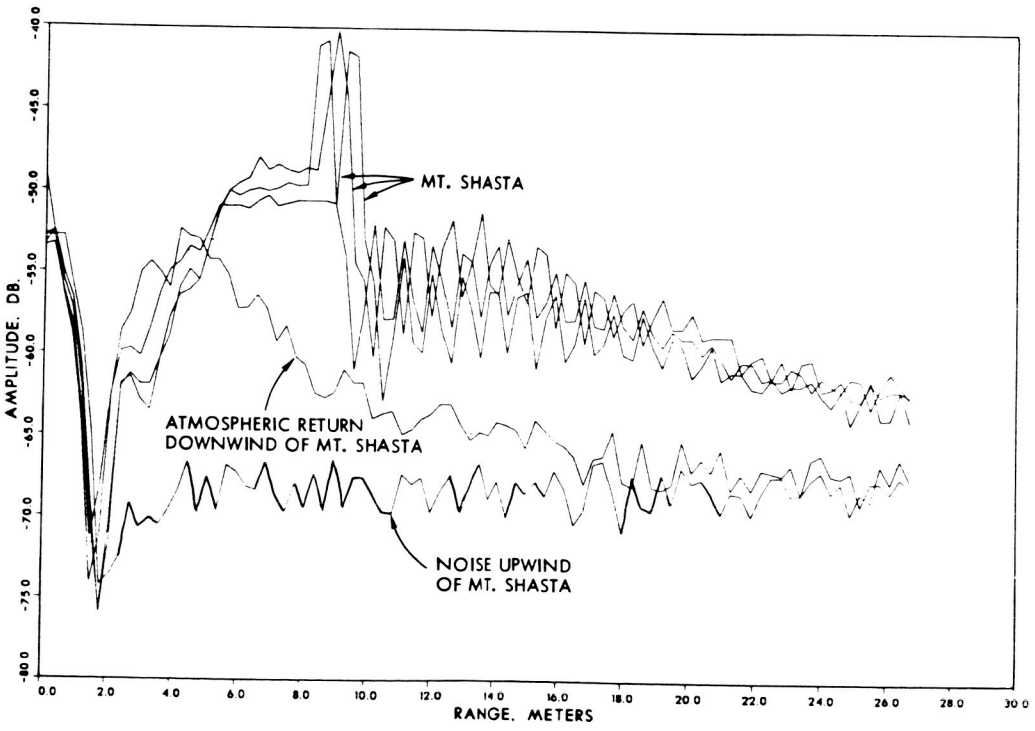

Figure 4. AMPLITUDE RETURN IN THE VICINITY OF A MOUNTAIN AFTER MODULATOR FAILURE.

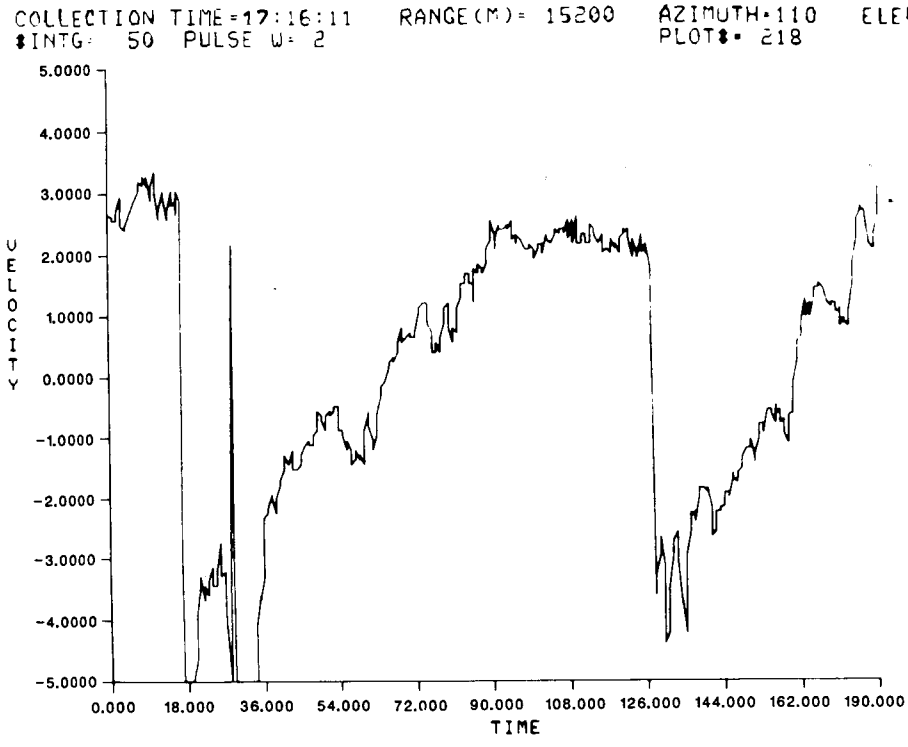

Figure 5. APPARENT DOPPLER VELOCITY OF A MOUNTAIN AT A RANGE OF 15 KM WITH ISOLATOR REMOVED.

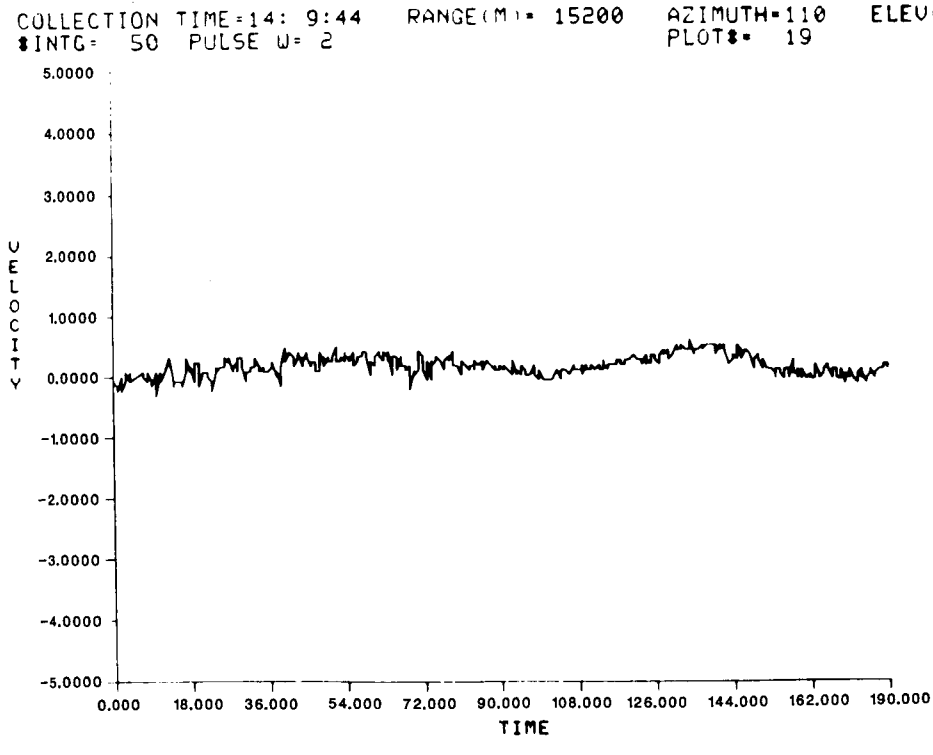

Figure 6. APPARENT DOPPLER VELOCITY OF A MOUNTAIN AT A RANGE OF 15 KM WITH ISOLATOR IN PLACE.

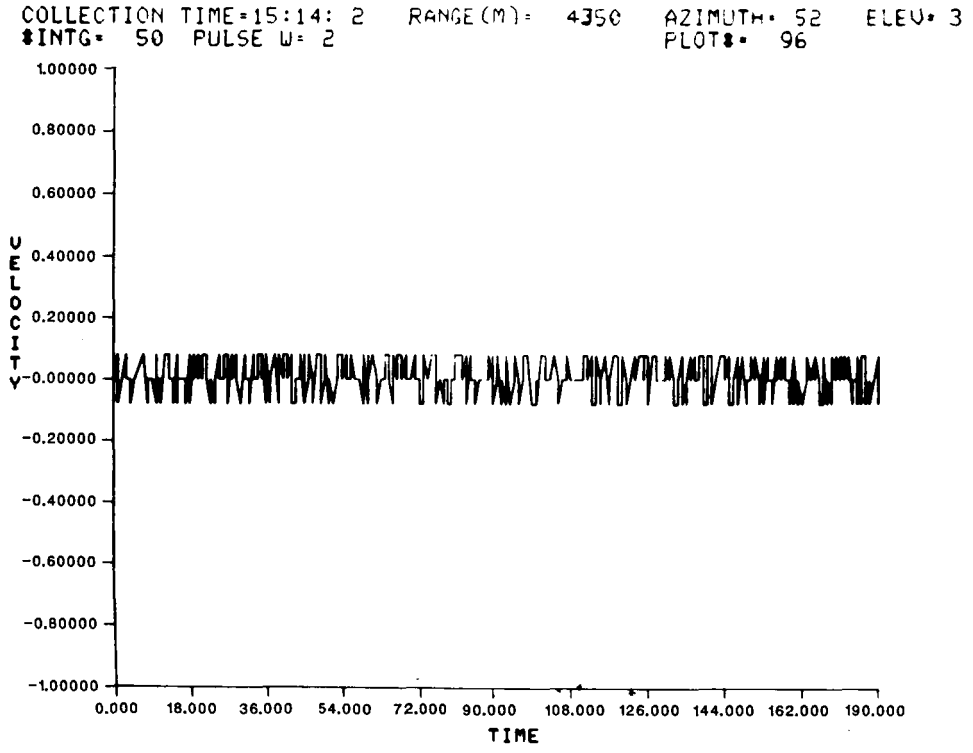

Figure 7. APPARENT DOPPLER VELOCITY OF A MOUNTAIN AT A RANGE OF 4 KM.

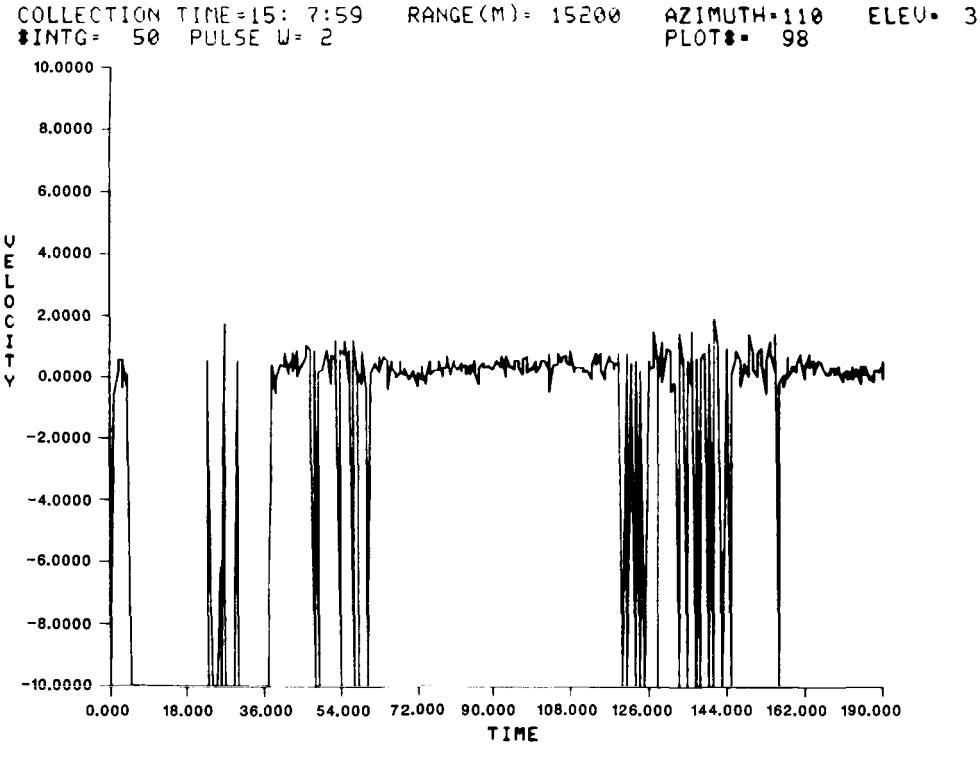

Figure 8. EFFECTS OF MOMENTARY LOSS OF LOCK ON VELOCITY MEASUREMENT.

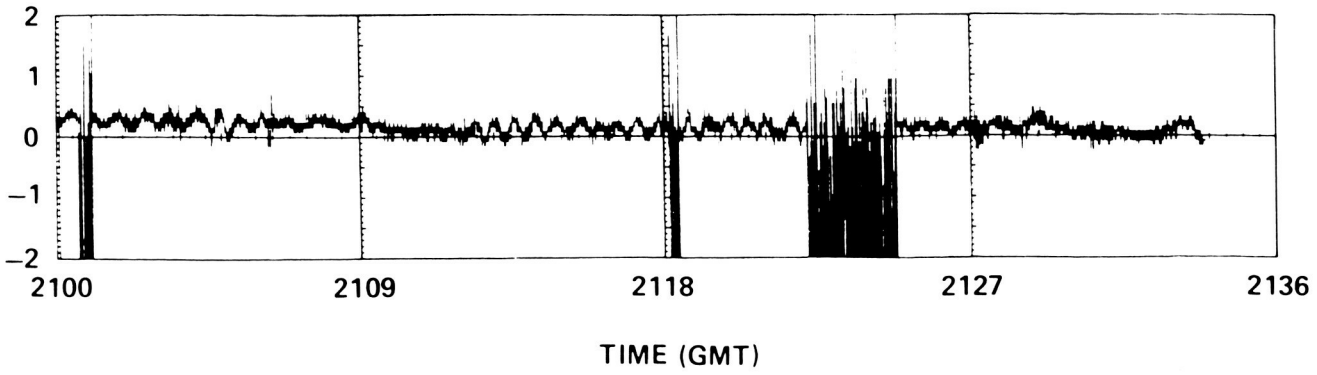

Figure 9. LONG-TERM STABILITY OF VELOCITY MEASUREMENT AGAINST A STATIONARY TARGET.

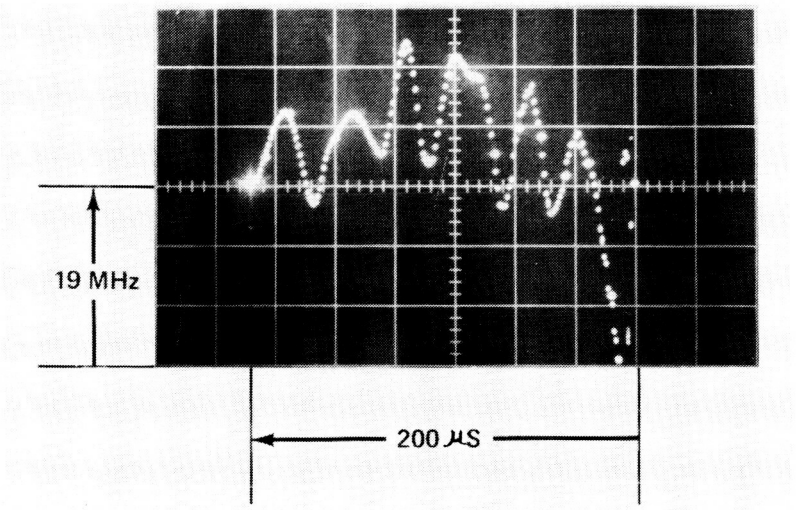

Figure 10. FREQUENCY EXCURSION OF MASTER OSCILLATOR LASER BEING DRIVEN OUT OF THE PASS BAND OF THE SIGNAL PROCESSOR ELECTRONICS.

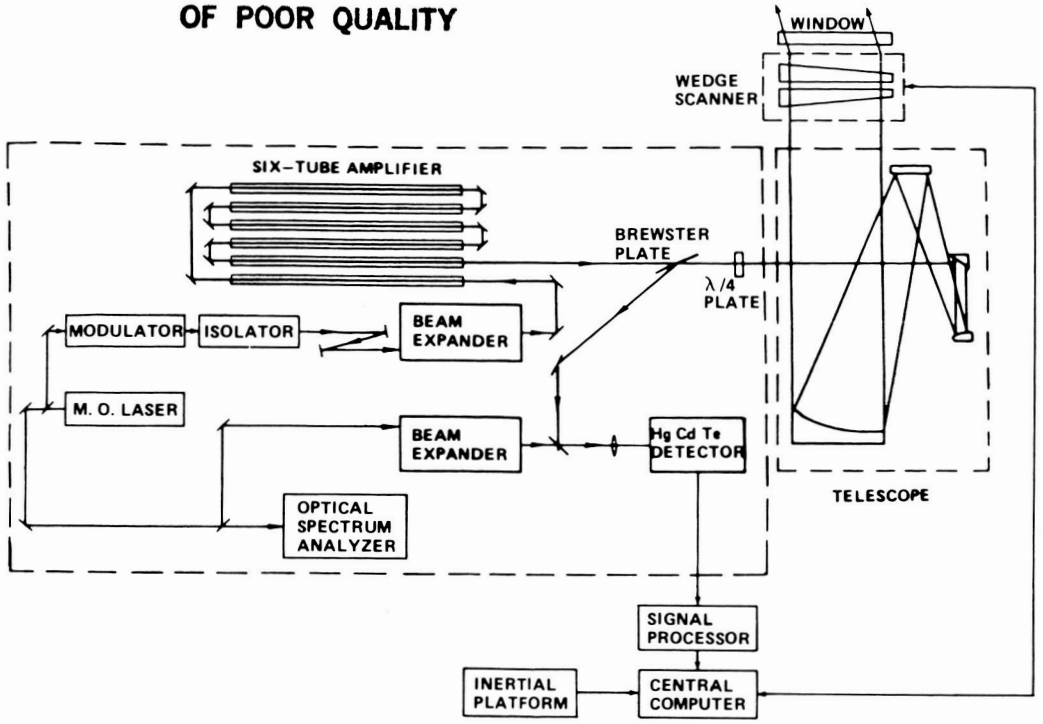

Figure 11. SIMPLIFIED BLOCK DIAGRAM OF AIRBORNE CONFIGURATION.

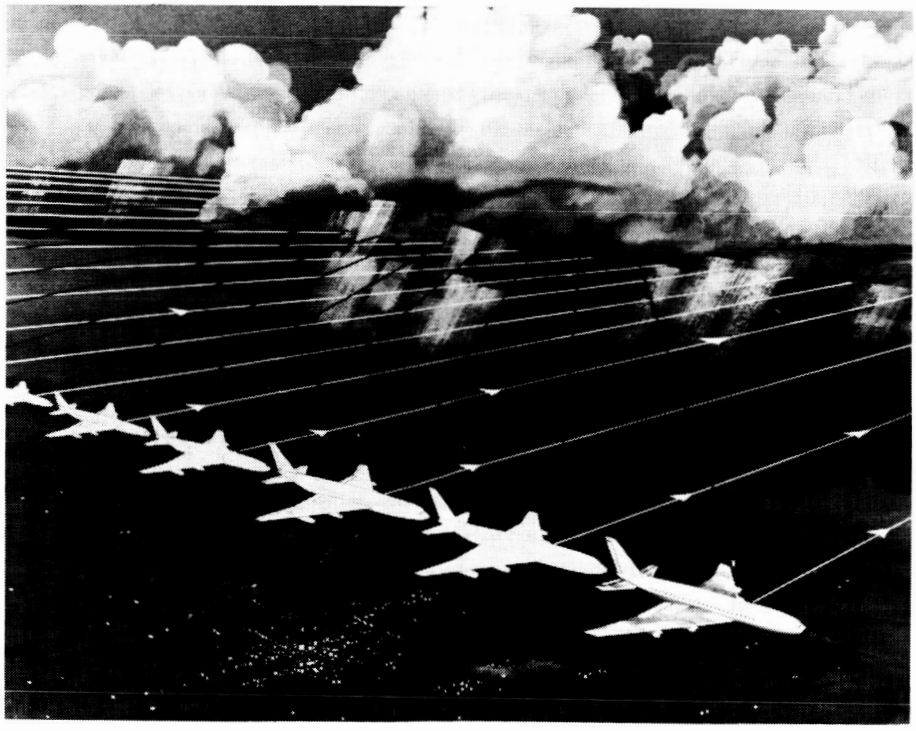

Figure 12. SCAN PATTERN OF THE AIRBORNE LIDAR.

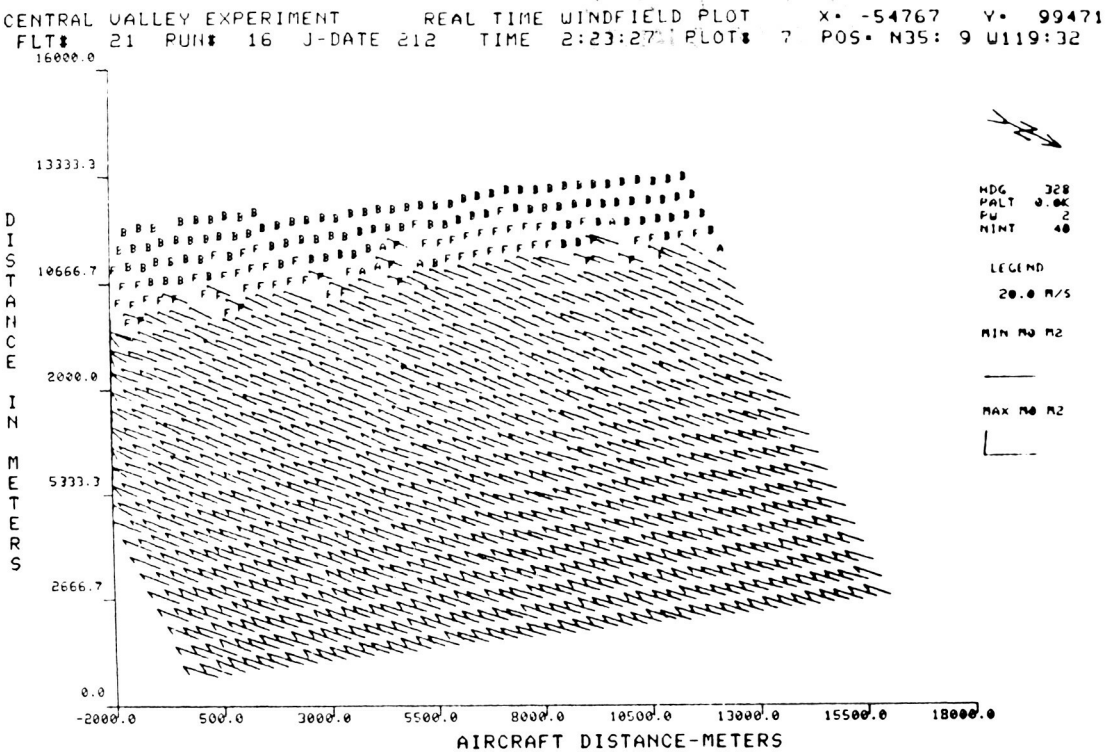

Figure 13. VECTOR VELOCITY MAP OF A UNIFORM FLOW FIELD IN A HORIZONTAL PLANE AT THE ALTITUDE OF THE AIRCRAFT.

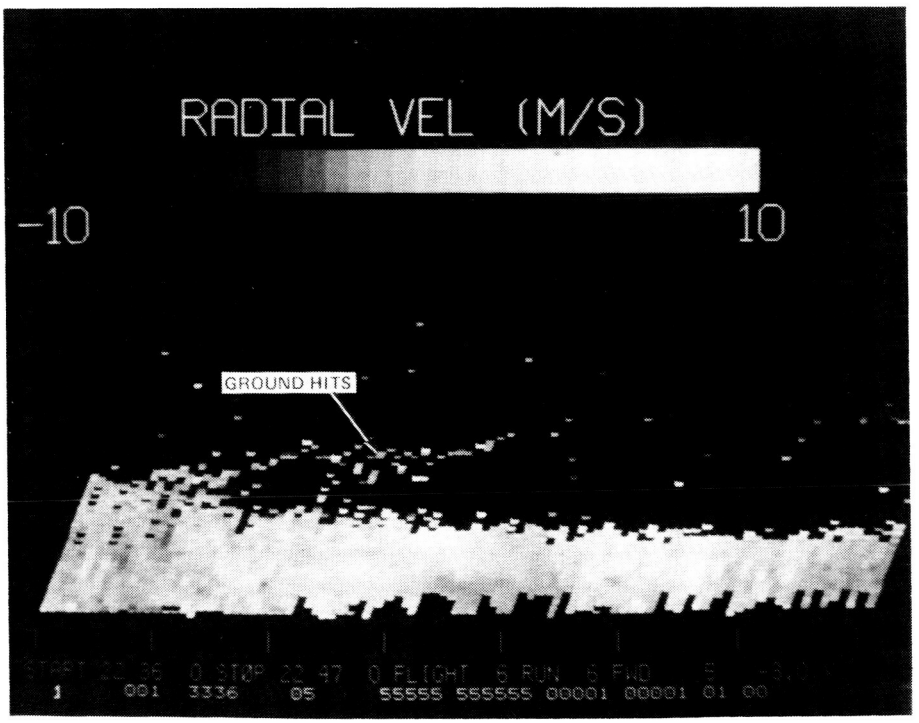

Figure 14. PLAN VELOCITY DISPLAY OF AIRBORNE MEASUREMENTS SHOWING GROUND RETURN FROM ADJACENT FORWARD SCANS HAVING AN ANGLE OF DEPRESSION OF 3 DEGREES.

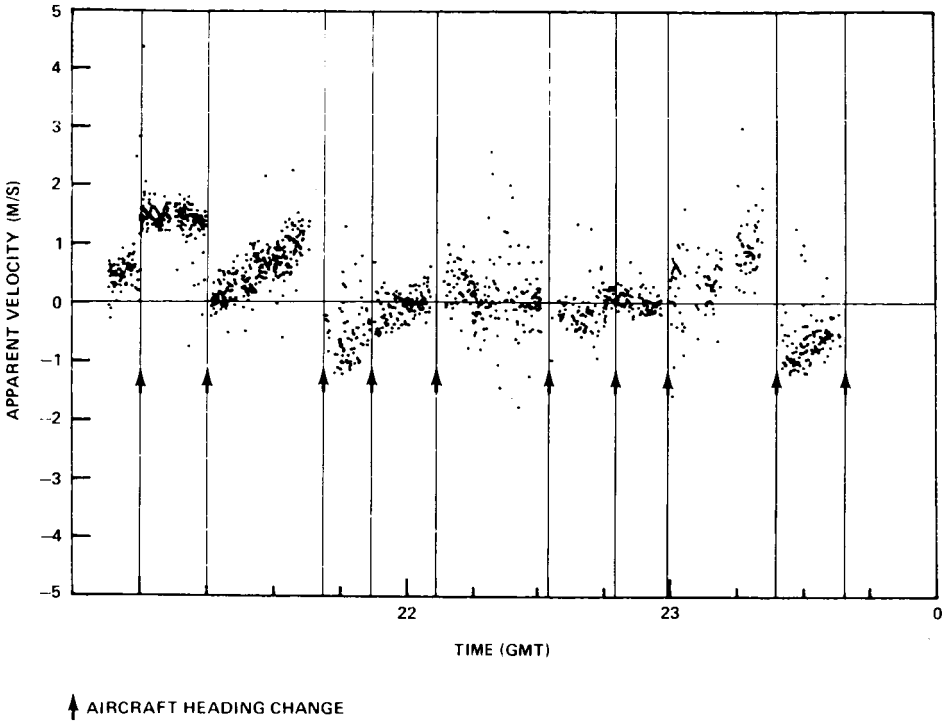

Figure 15. APPARENT DOPPLER VELOCITY OF GROUND AS A FUNCTION OF TIME.

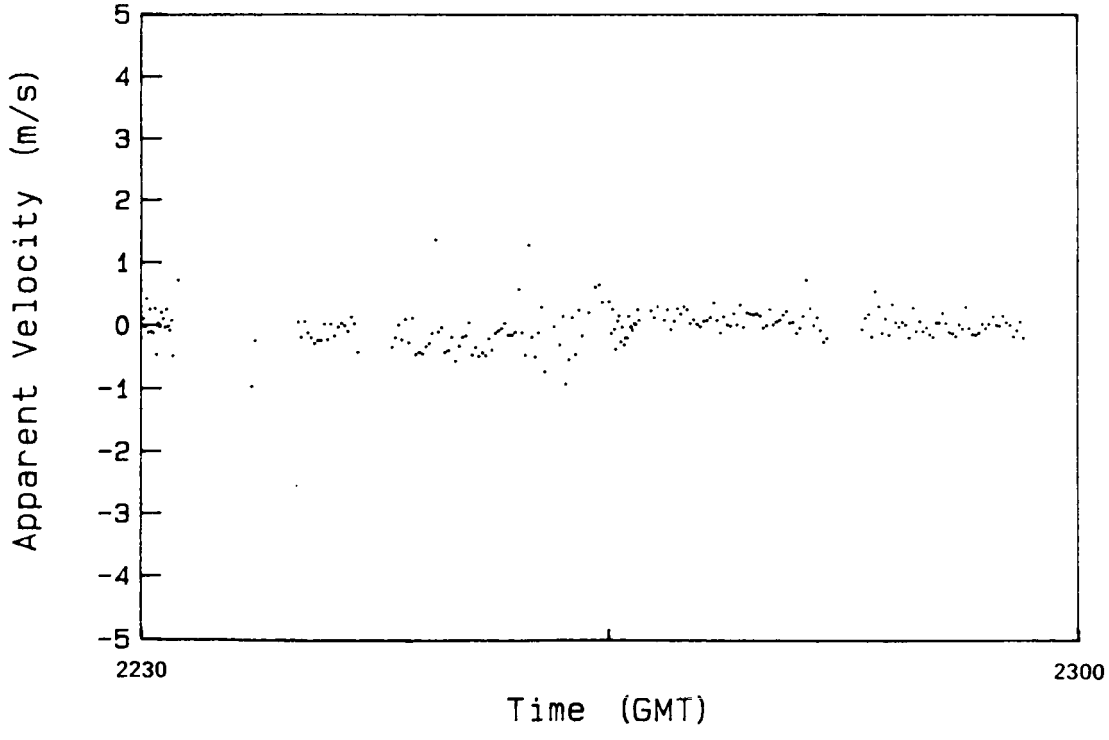

Figure 16. EXPANDED VIEW OF APPARENT DOPPLER VELOCITY OF GROUND AS A FUNCTION OF TIME.